DE GRUYTER OPEN
1862
RIGA TECHNICAL UNIVERSITY

Transport and Aerospace Engineering

ISSN 2255-9876 (online)
ISSN 2255-968X (print)
August 2017, vol. 4, pp. 80–87
doi: 10.1515/tae-2017-0010
https://www.degruyter.com/view/j/tae

Plotting the Flight Envelope of an Unmanned Aircraft System Air Vehicle

Nikolajs Glīzde

Institute of Aeronautics, Faculty of Mechanical Engineering, Transport and Aeronautics, Riga Technical University, Riga, Latvia

***Abstract* – The research is focused on the development of an Unmanned Aircraft System. One of the design process steps in the preliminary design phase is the calculation of the flight envelope for the Unmanned Aircraft System air vehicle. The results obtained will be used in the further design process. A flight envelope determines the minimum requirements for the object in Certification Specifications. The present situation does not impose any Certification Specification requirements for the class of the Unmanned Aircraft System under the development of the general European Union trend defined in the road map for the implementation of the Unmanned Aircraft System. However, operation in common European Aerospace imposes the necessity for regulations for micro class systems as well.**

***Keywords* – Aircraft design, flight envelope, loads, unmanned aircraft system.**

I. Introduction

There are several types of aircraft flight load diagrams, every of which usually is a variation of a flight parameter in relation to another parameter. Flight envelopes are calculated and constructed by engineers and applied by flight crews and pilots. During a flight, pilots use several plots and graphs. The four most important of them are:

1. Aircraft lift coefficient and Mach number variation (C_l–M);
2. Airspeed and flight altitude variation (V–h);
3. Aircraft centre of gravity and weight variation (X_{cg}–W);
4. Airspeed and load variation (V–n).

The most important of the above mentioned diagrams is the airspeed and load variation diagram (V–n). This diagram depicts the aircraft's limit loads as a function of airspeed. This diagram is very important mainly due to a maximum load factor which is obtained from the graph and used in the aircraft structural design. If the maximum load factor is insufficiently evaluated and calculated too low, the aircraft cannot withstand safely flight loads – is not airworthy. It is recommended for engineers to recalculate the V–n diagram several times during the design process for safety reasons [3], [5], [6], [10].

The Unmanned Aircraft System air vehicle flight envelope is plotted according to the parameters obtained during the conceptual design phase and the calculations in the preliminary design phase (see Table I).

TABLE I
PARAMETERS OF UNMANNED AIRCRAFT SYSTEM AIR VEHICLE

Parameter		value
Air vehicle mass	m	7.066 kg
Wing gross area	S_{wga}	0.98 m^2
Wing maximum lift coefficient, positive	C_{lmax}	1.6
Wing maximum lift coefficient, negative	$-C_{lmax}$	–0.8
Zero-lift-drag coefficient	C_{D0}	0.024482
Wing aspect ratio	AR	12
Angle of attack during gust	a	1.5464 rad^{-1}

Stall speed	V_S	8.5 m/s
Cruise speed	V_C	26 m/s
Maximum speed	V_{max}	33.8 m/s
Gravitational acceleration	g	9.81 m/s^2

The combined *V–n* diagram is constructed in three steps:

1. Basic *V–n* diagram;
2. Gust *V–n* diagram;
3. Combined *V–n* diagram.

The figure below shows the general shape of the *V–n* diagram [3], [5], [6], [10], [13], [16], [18], [20].

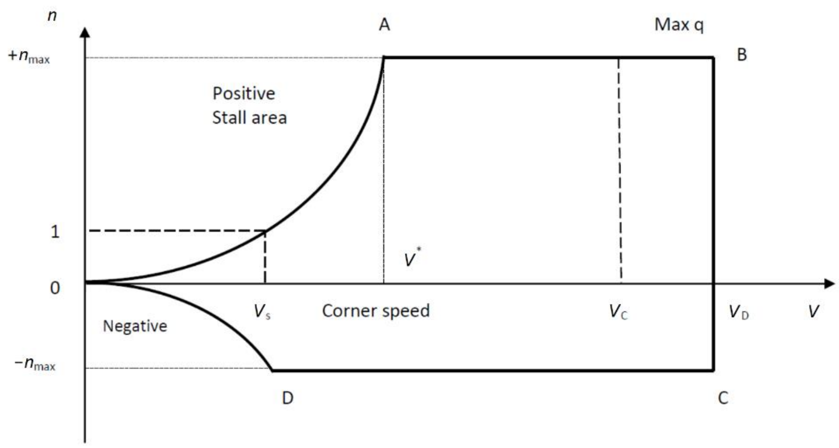

Fig. 1. The general shape of the *V–n* diagram.

II. FLIGHT ENVELOPE CONSTRUCTION

2.1. Basic V–n Diagram

The *V–n* diagram calculations involve the use of limit values and equations from the European Aviation Safety Agency Certification Specification for Very Light Aeroplanes CS-VLA [1], [2], [7], [8], [20]. This Certification Specification covers airworthiness requirements for Very Light Aircraft with a maximum certificated take-off weight of not more than 750 kg. Such regulations are not yet developed for micro class unmanned aircraft systems, which means that the above mentioned requirements should be taken as a basis [9], [11], [12].

The load on the aircraft on land is formed by the gravitational force which is 1*g*. The aircraft in flight is influenced by other loads one of which is acceleration. The load is usually defined as a load factor $n \cdot g$. In other words, the load on the aircraft is defined as a load of multiple gravitational acceleration *g*. The load factor is a ratio (1) between lift force and weight [3], [5], [6], [10], [13], [16] – [20]:

$$n = \frac{L}{W}, \quad (1)$$

where

L is lift force;

W is weight.

From [1] CS-VLA 335 it follows that the maximum cruise speed cannot be less than:

$$V_C = 2.4\sqrt{(mg)/S} = 20.19 =\sim 20.20\text{m/s}, \quad (2)$$

where

W/S is wing loading equal to 70.805 N/m^2, the value of which is obtained during wing and engine sizing calculations.

The requirement of CS is satisfied because the design requirement for the cruise speed is V_C = 26 m/s. In flight envelope calculations, the value of cruise speed calculated by (2) will be used to design a lighter air vehicle structure. The value will be reviewed in later design stages if necessary [3], [5], [6], [10], [13], [16], [18], [20].

The maximum cruise speed [3], [15] is:

$$V_{\max} = 1.3V_C = 26.26\text{m/s}. \tag{3}$$

According to [1], [2], [7], [8], [20] CS-VLA, the following load limits are determined:

n_{pos} = 3.8 maximum positive load limit;

n_{neg} = –0.5n_{pos}= –1.9 maximum negative load limit.

The aircraft dive speed [1], [4], [15] is:

$$V_d = 1.4V_C = 28.28\text{m/s} \tag{4}$$

Now the coordinates for points F and G can be set, which respectively are (V_d; 3.8) and (V_d; – 1.9).

To find coordinates for points A, B, J, K, it is necessary to calculate two equations in respect to coefficient $C_{l\max}$. The stall speed is calculated in accordance with the following equation:

$$V_S = \sqrt{\frac{2mg}{\rho_{SL} S_{wga} C_{L_{\max}}}} = 8.4956\,\text{m/s} \tag{5}$$

The recalculated stall speed almost matches with the design requirement stall speed. Therefore, in the further flight envelope calculations, the initial stall speed value will be used, in relation to coordinate point A (8.5, 1).

The upper curve or the load coefficient and speed function is:

$$n = \frac{L}{W} = \frac{0.5\rho_{SL} V^2 S_{wga} C_{L_{\max}}}{W} = 0.013855 \times V^2 \tag{6}$$

From the equation (6) and knowing maximum load n_{pos} (3.8), a speed in the point B, which is also the manoeuvring speed, can be calculated:

$$V = \sqrt{\frac{n}{0.013855}} = 16.56\,\text{m/s}. \tag{7}$$

Accordingly the coordinates for the point B are (16.56, 3.8).

In the same way, the equation for the lower curve is formed:

$$V_{Si} = \sqrt{\frac{-2mg}{\rho_{SL} S_{wga} \left(-C_{L_{\max}}\right)}} = 12.015\,\text{m/s}, \tag{8}$$

where

ρ_{SL} is air density at sea level.

Then the coordinates for the point K are (12.015; –1).

The lower curve or the load coefficient and speed function is:

$$-n = \frac{-L}{W} = \frac{0.5\rho_{SL} V^2 S_{wga}\left(-C_{L_{\max}}\right)}{W} = -0.006928 \times V^2 \tag{9}$$

From the equation (10) and knowing the maximum load n_{neg} (–1.9), a speed in the point J can be calculated:

$$V=\sqrt{\frac{-n}{-0.006928}}=16.56\,\mathrm{m/s}\,. \qquad (10)$$

The coordinates for the point J are (16.56; –1.9).

From the above calculations, the coordinates for points A, B, F, G, J and K have been obtained. Then the basic *V–n* diagram can be plotted:

O (0; 0)
A (8.5; 1)
B (16.56; 3.8)
F (28.28; 3.8)
G (28.28; –1.9)
J (16.56; –1.9)
K (12.015; –1)

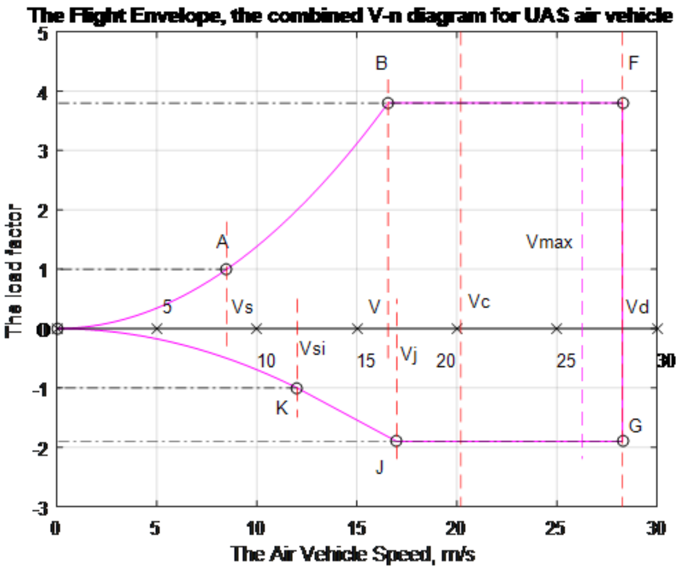

Fig. 2. Basic *V–n* diagram.

2.2. Gust V–n Diagram

The equation for the load coefficient variation as a function of the airspeed:

$$n=1+\frac{K_g V_{ge} V_e a \rho S_{wga}}{2W}\,, \qquad (11)$$

In accordance with [1], [2], [7], [8], [20] CS-VLA 333, the gust diagram is calculated for positive upward gusts and negative downward gusts for the cruise speed V_C and dive speed V_D. The gust speed is statistically measured and accordingly assumed for the aircraft V_D speed equal to 7.5 m/s and, V_C speed equal to 15.25 m/s.

2.2.1. Aircraft Load at Sea Level

In the preliminary design phase, the wing aspect ratio was determined: AR =12 [19]. The equation for the wing aspect ratio calculation is:

$$AR=\frac{b}{C}\,, \qquad (12)$$

where
b is wing span;
C is wing chord.

The equation for the wing mean geometric chord is:

$$C_{\text{mgc}} = \frac{S_{\text{wga}}}{b}. \tag{13}$$

Assuming that the wing is tapered and swept, (12) should be inserted into (13) yielding the following result:

$$b = \sqrt{AR \cdot S_{wga}} = 3.429\text{m}. \tag{14}$$

As the calculated wing span exceeds the functionally required length, it is recalculated with a newly defined aspect ratio value $AR = 8$:

$$b = \sqrt{AR \cdot S_{wga}} = 2.8\text{m}, \tag{15}$$

which satisfies the functional requirements.

The wing mean geometric chord according to (13) is:

$$C_{mgc} = \frac{S_{wga}}{b} = 0.35\text{m}. \tag{16}$$

The air vehicle mass aspect ratio is:

$$\mu_g = \frac{2 \cdot m}{\rho \cdot C_{mgc} \cdot ac \cdot S_{wga}} = 21.7496. \tag{17}$$

The gust alleviation factor is:

$$K_{\text{g}} = \frac{0.88\mu_{\text{g}}}{5.3 + \mu_{\text{g}}} = 0.7076. \tag{18}$$

In accordance with the equation (11), the gust load factor during cruise speed flight is:

$$n = 1 + \frac{0.7076(\pm 15.25)V_{\text{C}} \cdot 1.5464 \cdot 1.225 \cdot 0.98}{2 \cdot 69.32} = 1 \pm 0.1445 V_{\text{C}}. \tag{19}$$

From the equation above it follows:
positive value $n = 1 + 0.1445 \cdot 20.20 = 3.92$, and
negative value $n = 1 - 0.1445 \cdot 20.20 = -1.92$.

The same calculation is performed for the dive speed:

$$n = 1 + \frac{0.7076(\pm 7.5)V_{\text{D}} \cdot 1.5464 \cdot 1.225 \cdot 0.98}{2 \cdot 69.32} = 1 \pm 0.07106 V_{\text{D}}. \tag{20}$$

From the equation above it follows:
positive value $n = 1 + 0.07106 \cdot 28.28 = 3.01$, and
negative value $n = 1 - 0.07106 \cdot 28.28 = -1.01$.

2.2.2. Aircraft Load at a Cruising Altitude of 350 m Above Sea Level

The air density at an altitude of 350 m above sea level is 1.184 kg/m^3.

In accordance with (17), the air vehicle mass aspect ratio is:

$$\mu_{\text{g}} = \frac{2 \cdot 7.066}{1.184 \cdot 0.35 \cdot 1.5464 \cdot 0.98} = 5.5235. \tag{21}$$

The gust alleviation factor in accordance with (18) is:

$$K_g = \frac{0.88 \cdot \mu_g}{5.3 + \mu_g} = 0.44908 . \qquad (22)$$

The gust load factor in accordance with (11) during a cruise speed flight respectively is:

$$n = 1 + \frac{0.44908(\pm 15.25)V_C \cdot 1.5464 \cdot 1.184 \cdot 0.98}{2 \cdot 69.32} = 1 \pm 0.088635 V_C . \qquad (23)$$

From the equation above it follows:
positive value $n = 1 + 0.088635 \cdot 20.20 = 2.79$, and
negative value $n = 1 - 0.088635 \cdot 20.20 = -0.79$.
The same calculation is performed for the dive speed:

$$n = 1 + \frac{0.44908(\pm 7.5)V_D \cdot 1.5464 \cdot 1.184 \cdot 0.98}{2 \cdot 69.32} = 1 \pm 0.04359 V_D . \qquad (24)$$

From the equation above it follows:
positive value $n = 1 + 0.04359 \cdot 28.28 = 2.23$, and
negative value $n = 1 - 0.04359 \cdot 28.28 = -0.23$.

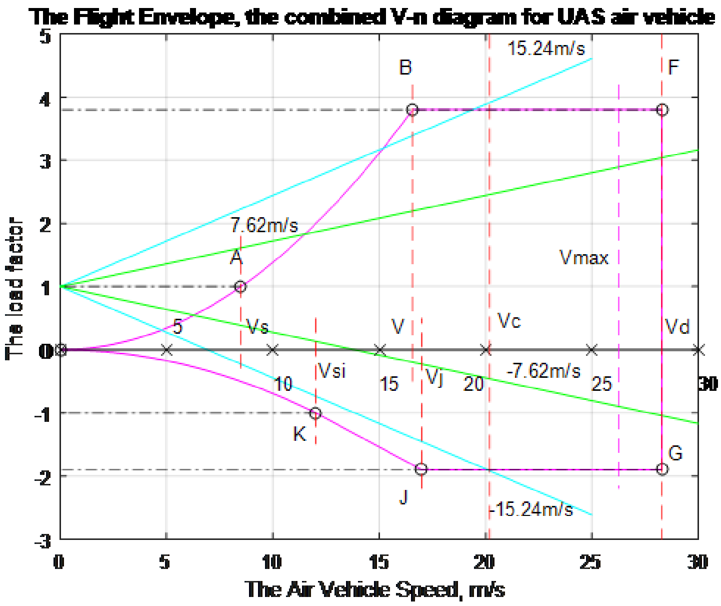

Fig. 3. Basic *V–n* diagram with gust lines.

Comparing the results from both parts, it is possible to conclude that the load factor at sea level is greater. Consequently, the following gust load factor values are taken for further calculations:
$n_{posg} = 3.92$
$n_{negg} = -1.92$
Thus, the coordinates for the points D and I are as follows: D (20.20; 3.92) and I (20.20; –1.92).

2.3. Combined V–n Diagram

The combined *V–n* diagram is plotted from the basic diagram and gust line intersection points.

In accordance with [1], [2], [7], [8], [20] CS-VLA 333, the gust load varies linearly between the speeds V_C and V_D.

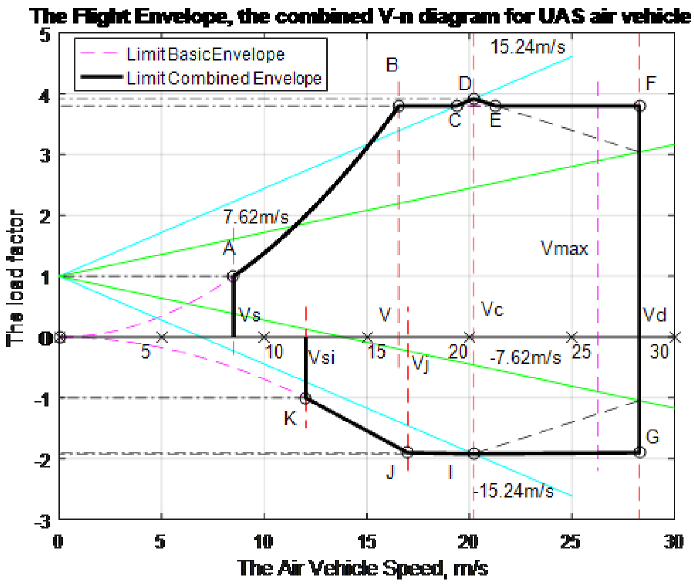

Fig. 4. Combined *V*–*n* diagram.

III. Conclusion

The analysis of the flight envelope makes it possible to conclude that gust loads do not create much greater loads on the air vehicle structure. This is feasible, because the micro class unmanned aircraft system is rather small in size, and the gust will most probably transfer the whole air vehicle structure.

References

[1] Certification Specifications, CS-VLA, European Aviation Safety Agency, 2009, [Online]. Available: www.easa.europa.eu.
[2] Certification Specifications, CS-23, European Aviation Safety Agency, 2015, [Online]. Available: www.easa.europa.eu.
[3] N. Ludovic, *Aircraft Structures Design Example*. University of Liège, 2014.
[4] M. Sadraey, *Aircraft Performance Analysis*. VDM Verlag Dr. Müller, 2009.
[5] E. C. T. Lanand and J. Roskam, *Airplane Aerodynamics and Performance*. DAR Corporation, 2003.
[6] L. J. Bertin and R. M. Cummings, *Aerodynamics for Engineers*, 5th ed. Pearson/Prentice Hall, 2009.
[7] Federal Aviation Regulations, Part 23, Airworthiness Standards: Normal, Utility, Aerobatic, and Commuter Category Airplanes, Federal Aviation Administration, Department of Transportation, Washington, 2011.
[8] Federal Aviation Regulations, Part 25, Airworthiness Standards: Transport Category Airplanes, Federal Aviation Administration, Department of Transportation, Washington, 2011.
[9] B. L. Stevens and F. L. Lewis, Aircraft Control and Simulation, 2nd ed. Wiley-VCH Verlag GmbH, 2003.
[10] J. Roskam, *Airplane Flight Dynamics and Automatic Flight Control*. DAR Corporation, 2007
[11] D. Mclean, *Automatic Flight Control Systems*. Prentice-Hall, 1990.
[12] R. Nelson, *Flight Stability and Automatic Control*. McGraw Hill, 1989.
[13] B. W. McCormick, *Aerodynamics, Aeronautics and Flight Mechanics*. Wiley-VCH Verlag GmbH, 1979.
[14] B. Etkin and L. D. Reid, *Dynamics of Flight-Stability and Control*, 3rd ed. Wiley-VCH Verlag GmbH., 1996.
[15] M. Sadraey and R. Colgren, “Derivations of major coupling derivatives, and the state space formulation of the coupled equations of motion,” *6th AIAA Aviation Technology, Integration and Operations Conference (ATIO)*, Wichita, KS, September 25–27, AIAA-2006-7790, 2006. https://doi.org/10.2514/6.2006-7790
[16] J. Roskam, *Airplane Design*. DAR Corporation, 2003.
[17] A. Urbahs and I. Jonaite, “Features of the use of unmanned aerial vehicles for agriculture applications”, Aviation, 2013, vol. 17, issue 4, pp. 170-175, 2013. https://doi.org/10.3846/16487788.2013.861224
[18] A. Urbahs, V. Petrovs, M. Urbaha, and K. Carjova, “Evaluation of functional landing and taking off characteristics of the hybrid aircraft in comparison with competing hybrid air vehicles,” in *Transport Means – Proceedings of the International Conference*, Kaunas, 24–25 October, 2013, pp. 246–249.
[19] P. Jackson, *Jane’s All the World’s Aircraft*. Jane’s Information Group, 1996–2011.
[20] Joint Aviation Requirements, CS-25, Large Airplanes, European Aviation Safety Agency, 2007.

Nikolajs Glīzde obtained a degree of Bachelor of Technical Sciences in 1993 and a professional degree of Automotive Enterprises Engineer in 1994. He received a degree of Master of Transport Systems Engineering in 2011. The Author began studies for a Doctoral degree in 2015.
For the last fifteen years the author has been working as a technical specialist. His work is related to military vehicles of different types.
The author's current interests of research refer to the development of Unmanned Aircraft Systems, as the integration of Unmanned Aircraft Systems in common European Aerospace is the latest European trend which requires research and development in different technological fields.
Address: Institute of Aeronautics, Faculty of Mechanical Engineering, Transport and Aeronautics, Riga Technical University, Lomonosova 1A, k-1, Riga, LV-1019, Latvia.
Phone: +371 67089990
E-mail: nikolajs.glizde@rtu.lv